**Atmospheric
Chemistry
and Physics
Discussions**

Interactions of meteoric smoke particles with sulphuric acid in the Earth's stratosphere

R. W. Saunders[1], S. Dhomse[2], W. S. Tian[3], M. P. Chipperfield[2], and J. M. C. Plane[1]

[1]School of Chemistry, University of Leeds, Leeds LS2 9JT, UK
[2]School of Earth and Environment, University of Leeds, Leeds LS2 9JT, UK
[3]College of Atmospheric Sciences, Lanzhou University, Lanzhou 730000, China

Correspondence to: J. M. C. Plane (j.m.c.plane@leeds.ac.uk)

ACPD

12, 1553–1584, 2012

Interactions of meteoric smoke particles with sulphuric acid

R. W. Saunders et al.

Title Page

Abstract	Introduction
Conclusions	References
Tables	Figures

|◄ | ►|

◄ | ►

Back | Close

Full Screen / Esc

Printer-friendly Version

Interactive Discussion

Abstract

Nano-sized meteoric smoke particles (MSPs) with iron-magnesium silicate compositions, formed in the upper mesosphere as a result of meteoric ablation, may remove sulphuric acid from the gas-phase above 40 km and may also affect the composition and behaviour of supercooled H_2SO_4-H_2O droplets in the global stratospheric aerosol (Junge) layer. This study describes a time-resolved spectroscopic analysis of the evolution of the ferric (Fe^{3+}) ion originating from amorphous ferrous (Fe^{2+})-based silicate powders dissolved in varying Wt % sulphuric acid (30–75 %) solutions over a temperature range of 223–295 K. Complete dissolution of the particles was observed under all conditions. The first-order rate coefficient for dissolution decreases at higher Wt % and lower temperature, which is consistent with the increased solution viscosity limiting diffusion of H_2SO_4 to the particle surfaces. Dissolution under stratospheric conditions should take less than a week, and is much faster than the dissolution of crystalline Fe^{2+} compounds. The chemistry climate model UMSLIMCAT (based on the UKMO *Unified Model*) was then used to study the transport of MSPs through the middle atmosphere. A series of model experiments were performed with different uptake coefficients. Setting the concentration of 1.5 nm radius MSPs at 80 km to 3000 cm^{-3} (based on rocket-borne charged particle measurements), the model matches the reported Wt% Fe values of 0.5–1.0 in Junge layer sulphate particles, and the MSP optical extinction between 40 and 75 km measured by a satellite-borne spectrometer, if the global meteoric input rate is about 20 t d^{-1}. The model indicates that an uptake coefficient ≥ 0.01 is required to account for the observed two orders of magnitude depletion of H_2SO_4 vapour above 40 km.

1 Introduction

The acidic weathering of ferrous (Fe^{2+})-based silicate minerals such as olivines ($Mg_{2x}Fe_{2-2x}SiO_4$) and pyroxenes ($Mg_xFe_{1-x}SiO_3$, where $0 \leq x \leq 1$) is an important pathway to the formation of secondary minerals on Earth (Loughnan, 1969; White,

1995). The weathering process is complex and involves dissolution and oxidation steps, but studies indicate that the Fe-rich olivine/pyroxene structures are more soluble at low temperatures and weather faster than Fe-poor or non-Fe minerals (Siever and Woodford, 1979). Similar processes also occur on Mars, but under very different

5 chemical conditions (Burns, 1993; Hurowitz et al., 2006), and are also likely to lead to stabilised hydrated and sulphate-complexed ferric (Fe^{3+}) ion species in the Martian permafrost (Burns, 1987). Amorphous silicate structures are the leading candidates for meteoric smoke particles or MSPs (Hervig et al., 2009; Saunders and Plane, 2011). These are nanoparticles formed by the recondensation of primarily Fe, Mg and Si ox-

10 ide species resulting from the ablation of meteoroids passing through planetary upper atmospheres (Plane, 2003).

MSPs have been detected in the Earth's upper atmosphere by rocket-borne and radar techniques (see, e.g. Rapp et al., 2007) which indicate typical total (neutral + charged) particle numbers of a few thousand per cm^{-3} above 75 km. More recently,

15 the first optical detection (at 1.037 μm) of MSPs between ∼ 40 and 80 km by satellite-borne spectrometry was used to infer the possible particle composition (Hervig et al., 2009). Satellite data has also been modelled to investigate the likely extent of optical extinction by MSPs between 30 and 40 km (Neely III et al., 2011).

MSPs are thought to participate in the nucleation of water-ice clouds in the meso-

20 sphere (Rapp and Thomas, 2006; Gumbel and Megner, 2009), and also impact on trace vapours such as H_2SO_4 and HNO_3 throughout the middle atmosphere (Turco et al., 1981; Prather and Rodriguez, 1988; Mills et al., 2005). After MSPs have been transported down from the mesosphere in the winter polar vortex (Curtius et al., 2005), they are thought to be assimilated in liquid (supercooled) H_2SO_4-H_2O droplets (typ-

25 ically 40–75 Wt% acid composition, radius > 100 nm) in the stratospheric aerosol or Junge layer which is located between 15 and 30 km in altitude (Carslaw et al., 1997; Deshler, 2008). These droplets can act as nuclei for polar stratospheric cloud (PSC) formation via uptake of water and nitric acid at temperatures below ∼ 210 K (Voigt et al., 2005).

Iron and magnesium of meteoric origin have been identified in positive ion spectra from droplets sampled in situ in the lower stratosphere (Murphy et al., 1998; Cziczo et al., 2001), with approximately half of the analysed particles reported to contain 0.5–1.0 Wt% of meteoric iron. Typical spectra of the sampled particles were closely repli-

5   cated by the dissolution of Fe and Mg compounds in a 65% (Wt) H_2SO_4 solution. At the low temperatures present in the stratosphere (180–240 K), the question of particle solubility is key in beginning to understand the composition of stratospheric aerosol, as the relative proportions of solid/solution phase metals in such aerosol are likely to control the freezing behaviour of the H_2SO_4-H_2O droplets (Wise et al., 2003). Previous

10 studies (e.g. Biermann et al., 1996) have concluded that meteoric material would not be an efficient seed for heterogeneous droplet freezing, but the chosen material used was not characteristic of the particle composition identified in stratospheric aerosol (Cziczo et al., 2001).

Balloon-borne mass spectroscopic measurements made in the 1980s e.g. (Arnold

15 et al., 1981; Viggiano and Arnold, 1981; Schlager and Arnold, 1987) delineate three distinct regions in the stratosphere where the concentration of gas-phase sulphuric acid varies significantly. Comparatively low concentrations, typically ranging between 10^4 and 10^5 cm^{-3} (outside of periods of major volcanic activity) are found below 30 km, where temperatures below 230 K result in the condensation of binary solutions of

20 H_2SO_4-H_2O to form stratospheric sulphate aerosol (SSA). Between 30 and 35 km, with increasing temperatures, the gas-phase concentration increases to 10^6–10^7 cm^{-3}. Above 35 km, measurements indicate a "turning-point", whereby concentrations begin to decrease up to $\sim$ 40 km. Above this altitude, data is restricted to a couple of balloon flights (Arijs et al., 1983, 1985), with H_2SO_4 levels at 45 km falling to $\sim 10^4$–10^5 cm^{-3}.

25 The reasons for an approximate two orders of magnitude depletion at 45 km (compared with the peak at $\sim$ 35 km) has long been the subject of debate, with gas-phase chemistry, photolysis and heterogeneous uptake on MSPs/metal atoms being proposed as possible processes (Turco et al., 1981; Vaida et al., 2003). A 1-D modelling study of MSP–acid interaction (Turco et al., 1981), where chemical neutralisation

Title Page

Abstract	Introduction
Conclusions	References
Tables	Figures

| ◄◄ | ►► |
| ◄ | ► |

Back | Close

Full Screen / Esc

Printer-friendly Version

Interactive Discussion

(resulting from metal atom-acid molecule collisions) was assumed, indicated that a downward metal atom flux of $5 \times 10^6 \, cm^{-2} \, s^{-1}$ from the upper mesosphere (equivalent to a global meteoric mass influx of $\sim 200 \, t \, d^{-1}$) was required to account for the observed depletion in H_2SO_4 at 45 km. However, this flux value lies significantly be-
yond the upper limit of what is now currently considered to be a likely range of between ~ 5 and $50 \, t \, d^{-1}$ (Vondrak et al., 2008). In addition, this model involved an arbitrary choice of collision rate scaling with which to determine the acid loss to smoke particles (Turco et al., 1981). A more recent 2-D modelling study of H_2SO_4 photolysis and sulphur gas and aerosol chemistry concluded that visible wavelength photolysis
($H_2SO_4 + h\nu \rightarrow SO_3 + H_2O$) via OH stretch excitation could not account for the loss of H_2SO_4 vapour above 40 km. With VUV photolysis of H_2SO_4 being too slow below 80 km, it was therefore suggested that irreversible loss to smoke particles, although not treated in their study, was the most likely cause of the observed gas-phase depletion above 40 km (Mills et al., 2005).

   This paper describes a combined laboratory and modelling study. The laboratory component measured the rates at which MSP analogue particles dissolve in concentrated H_2SO_4/H_2O solutions under stratospheric conditions. The modelling component explored the distribution of MSPs in the middle atmosphere, constrained by the available observations: rocket-borne particle detectors above 80 km (Gelinas et al., 2005;
Lynch et al., 2005), optical extinction between 40 and 80 km (Hervig et al., 2009), and the Fe wt% in Jungle layer droplets (Murphy et al., 1998; Cziczo et al., 2001). From this it was possible to constrain the uptake coefficient of H_2SO_4 on MSPs required to explain the observed decrease in concentration of this acid vapour above 40 km.

2 Acid dissolution of amorphous MSP analogues

2.1 Experimental technique

We conducted a series of experiments in which a sol-gel synthesised amorphous fay-
alite (Fe_2SiO_4) powder was dissolved in 30–75 Wt% acid solutions over a tempera-
ture range of 223–295 K. This composition was taken as a representative analogue
for MSPs (Saunders and Plane, 2006). Other mixed metal ($x > 0$) olivine and pyrox-
ene compositions are also likely in MSPs. We therefore also synthesised $MgFeSiO_4$,
$FeSiO_3$ and $MgFeSiO_3$ powders using the sol-gel process and studied their dissolution
characteristics over more limited temperature/acid Wt% ranges for comparison with the
fayalite powder. Particle dissolution and the Fe oxidation state were monitored spec-
troscopically to determine the rate and extent of particle solubility. The data was used
to determine reaction rate coefficients for specific temperature/acid Wt% combinations,
and then activation energies for the silicate powder dissolution process.

Amorphous powders of the iron ($x = 0$) end-members of the olivine (fayalite) and py-
roxene (ferrosilite) series, and mixed composition powders ($x \sim 0.5$) were synthesised
in accordance with procedures described by (Thompson et al., 1996). Briefly, solu-
tions of either sodium metasilicate (Na_2SiO_3) or orthosilicate (Na_4SiO_4) were mixed
in the desired stoichiometric amounts with 0.1 M solutions of $Fe[NH_4]_2(SO_4)_2 \cdot 6H_2O$
(Mohr's salt), or both Mohr's salt and $MgCl_2$ for the generation of mixed composition
powders. In each case, the gelatinous precipitate immediately formed was left for 1–
2 days, before excess liquid was decanted and the solids washed thoroughly to remove
any by-products. The remaining liquid was evaporated using a heating plate, and the
solids powdered using a pestle and mortar. The resulting powders were then stored in
a dessicator, prior to IR characterisation and then sulphuric acid dissolution studies.

Figure 1 shows a microscope image of the synthesised Fe-silicate particles, which
exhibit a range of shapes and of sizes from $\sim$ 1–50 µm (the applicability of particles
in this size range to MSPs is discussed below). Mid-IR spectra (4000–450 cm^{-1})
were taken directly from the solid samples using an FT-IR spectrometer (Spectrum

One, PerkinElmer) at a resolution of $1\,cm^{-1}$. All powders showed a broad, structureless peak between 800 and $1000\,cm^{-1}$, corresponding to the Si-O stretch observed in amorphous silicates (Draine, 2003). For subsequent analysis of reactions of synthesised silicate powders with sulphuric acid, weighed amounts (typically 5–10 mg) of the Fe and Fe-Mg silicate powders were placed in stoppered conical flasks with a total volume of 50 ml of a H_2SO_4 solution (98 %), diluted to a desired acid Wt% in deionised water. Solution spectra from 200–600 nm at a resolution of 1 nm were taken using a UV-visible spectrometer (Perkin Elmer-Lambda 900) with 1 cm quartz cuvettes, at regular time intervals. For experiments below room temperature, an immersion cooler (Neslab CC100) was used in combination with a methanol bath, in which the acid solution was equilibrated prior to addition of the sample powder and periodic extraction of aliquots for spectroscopic analysis. Due to the increasing solution viscosity at lower temperature and higher acid Wt%, it was necessary to allow solutions of $>50\,Wt\,\%$ at $T < 273\,K$ to stand for a 5–10 min period after removal from the bath, before spectra acquisition was possible.

2.2 Experimental results

Figure 2 shows a representative data set for the fayalite-acid solution experiments. The top panel shows the evolution with time of the UV-visible absorbance for $\lambda \leq 400$ nm (no absorbance was observed at longer wavelengths) for a 75 % Wt acid solution at 273 K, with 8.1 mg of the Fe_2SiO_4 powder added to give $[Fe^{2+}]_{t=0} \sim 7.9 \times 10^{-4}$ M in 50 ml of the acid solution. The data shows the increase in absorbance for peaks at 289 nm and 220 nm from the first spectrum taken 3 min after addition of the powder, to the final spectrum after 30 min, at which point no further increase in absorbance was observed.

The aqueous solution spectroscopy of Fe^{2+}/Fe^{3+} ions has been extensively studied. Whilst the Fe^{2+} ion exhibits only a small continuous absorbance (molar extinction $\varepsilon < 50\,l\,mol^{-1}\,cm^{-1}$) for $\lambda < 300$ nm (Potterill, 1936), the "bare" Fe^{3+} ion displays much greater ε values in this region (increasing to $>3000\,l\,mol^{-1}\,cm^{-1}$ for $\lambda < 250$ nm,

Whiteker and Davidson, 1953). However, in acidic solutions, hydration of the ion (in weak solutions) leads to the formation of the $Fe(OH)^{2+}$ species (absorbance peak at $\sim 300\,nm$ with $\varepsilon \sim 2500\,l\,mol^{-1}\,cm^{-1}$), whilst complexation with sulphate ions in strongly acidic solutions produces $Fe(SO_4)^+$ (peak at $\sim 302\,nm$, $\varepsilon \sim 2200\,l\,mol^{-1}\,cm^{-1}$), and

5    $Fe(SO_4)_2^-$ species, whose peak absorbance shifts to $\sim 290\,nm$ ($\varepsilon \sim 3000\,l\,mol^{-1}\,cm^{-1}$) at increasing acid solution strength (Wt%) (Whiteker and Davidson, 1953).

The spectra observed in Fig. 2 are therefore consistent with increasing absorption by the bare Fe^{3+} ion at 220 nm, and the $Fe(SO_4)_2^-$ complex ion at 289 nm. To determine the total final $[Fe^{3+}]$ in solution, an ε value of $4565\,l\,mol^{-1}\,cm^{-1}$ at 220 nm was

10   used (Scharf and Lee, 1962). The final absorbance value of 1.3 at 289 nm indicates a $[Fe^{3+}]_{complexed}$ of $4.3 \times 10^{-4}\,M$ ($= 1.3/3000$) or $\sim 55\%$ of $[Fe^{2+}]_{t=0}$, whilst $A_{max} = 1.61$ at 220 nm is consistent with a $[Fe^{3+}]_{bare} = 3.5 \times 10^{-4}\,M$ ($= 1.61/4565$) or $\sim 44\%$ of $[Fe^{2+}]_{t=0}$ to give a total $[Fe^{3+}]$ of $7.8 \times 10^{-4}\,M$. This indicates that, to within experimental error, complete conversion of solid-phase ferrous ion through to the ferric ion in

15   solution occurred.

The bottom panel of Fig. 2 shows the calculated values (solid triangles) of the ratio (α) of measured absorbance at time (t) to the final (maximum) value. In addition, the red line is a least squares optimised fit to the data points using an expression of the form;

20    $$\alpha = 1 - \exp(-kt) \tag{1}$$

where k (s^{-1}) is a single first-order rate coefficient which encompasses all reaction processes. These include: (i) H_2SO_4 diffusion to particle surfaces; (ii) oxidation of Fe^{2+} to Fe^{3+}; (iii) dissolution; and (iv) ion hydration/complexation in solution. For the 75 % Wt-273 K solution, k was determined to be $(5.6 \pm 0.3) \times 10^{-3}\,s^{-1}$.

25   Similar spectral data was acquired for 75 % Wt acid-fayalite powder solutions at $T = 223\,K$, 243 K, 263 K and 295 K, and for 30 %, 40 %, 50 % and 60 % Wt solutions at these same temperatures (except for the 30 % solution at 223 K, where solution freezing occurs), yielding k for each set of conditions. Experiments at temperatures below

223 K proved to be impractical due to the rapidly increasing viscosity of the solutions, as discussed below. In all cases (over different timescales), 100 % conversion of initial Fe^{2+} in the added fayalite powder sample to Fe^{3+} in solution was recorded. The main differences observed in experiments with varying acid solution strengths (at the same temperature) were: (i) a shift in the complexed ion peak from 289 nm (75 % solution) to ~ 300 nm (30 %); (ii) an increase in the ratio of the peak absorbance at 220 nm to the absorbance between 289–300 nm, from 1.3 to 1.9 as the %Wt decreased from 75 to 30 %, consistent with a final Fe^{3+} solution content of approximately equal amounts of bare and complexed ion; and (iii) a decrease in k at higher acid Wt %. Similarly, at constant acid Wt %, k decreased at lower temperatures, the complexed Fe^{3+} peak shifted to lower wavelength, and the peak absorbance ratio decreased. Qualitatively, the decrease in rate coefficient with decreasing temperature and increasing acid Wt % is consistent with increasing solution viscosity η (and hence H_2SO_4 diffusion coefficient) for these conditions. For example, η (75 % Wt) ~ 13 cP compared with η (30 % Wt) ~ 2 cP at 295 K; whilst at 223 K, η (75 % Wt) ~ 1450 cP compared with η (30 % Wt) ~ 50 cP (Williams and Long, 1995). That is, the diffusion coefficient ($D \alpha T / \eta$) of H_2SO_4 in a 75 % Wt solution at 223 K is ~ 150 times smaller than at 295 K, and 29 times smaller than for a 30 % Wt solution at 223 K. This compares with k decreasing between 295 and 223 K by factors of ~ 2700 (75 % Wt) and ~ 27 (30 %). For temperatures colder than those accessed in our experiments ($T < 223$ K), solution viscosity would rapidly increase e.g. η (75 % Wt) ~ 3.5×10^5 cP at 200 K, which should result in a corresponding further decrease in k.

Casting the temperature dependence of k at each Wt % solution in Arrhenius form (i.e., $\ln k$ versus $1/T$) yields the activation energy (E_a) and pre-exponential factor A. These are listed in Table 1 and can be used to calculate k (Wt % = 30–75 %, T = 223–295 K) and hence estimate the characteristic time for which any fraction of the initial Fe^{2+} in the fayalite powder will be converted into Fe^{3+}. Figure 3 is a contour plot showing the time taken in hours for 99.9 % of particle Fe^{2+} to be dissolved to Fe^{3+}, as a function of Wt % and T. Under the most "extreme" conditions (75 % acid/223 K)

amenable to spectroscopic analysis, the complete conversion of Fe^{2+} in particles to Fe^{3+} in solution takes ~ 128 h, i.e. 6 days. It should be stressed that these timescales are likely to represent upper limits for such a process involving "real" MSPs in the upper atmosphere, which typically are much smaller (below 20 nm in radius) than those used in our experiments. The laboratory production of such small nanoparticle sizes is not currently possible either through direct synthesis or by further grinding of micron-sized particle powders. At these small dimensions, higher surface area-to-volume ratios are likely to lead to enhanced initial uptake of acid molecules and dissolution (Hochella et al., 2008).

Experiments with the other synthesised powders ($MgFeSiO_4$ and $FeSiO_3/MgFeSiO_3$) showed that k was lower by a factor of 2–5 compared with Fe_2SiO_4 under comparable conditions i.e. longer times were required for the complete conversion to Fe^{3+} ions, which was nevertheless observed for all powders under all conditions. For example, at 273 K for 75 % Wt acid solutions, $k = 2.5 \times 10^{-3}\,s^{-1}$ ($MgFeSiO_4$), $3.0 \times 10^{-3}\,s^{-1}$ ($FeSiO_3$) and $1.2 \times 10^{-3}\,s^{-1}$ ($MgFeSiO_3$), compared with $5.6 \times 10^{-3}\,s^{-1}$ for Fe_2SiO_4. These trends are consistent with the reported slower dissolution behaviour, particularly at lower temperatures, of the more Fe-depleted olivines and of the pyroxene mineral series (Siever and Woodford, 1979; Burns, 1993; Stopar et al., 2006).

3 Modelling MSPs in the middle atmosphere

A 3-D Chemistry Climate Model (CCM) – UMSLIMCAT – was used to study the atmospheric transport of MSPs and the heterogeneous uptake of H_2SO_4. UMSLIMCAT is based on the UK Met Office Unified Model (UM) with a stratospheric chemistry scheme from the SLIMCAT model (Chipperfield, 2006). The CCM is described in detail elsewhere (Tian and Chipperfield, 2005). Briefly, the model has 64 vertical levels from the surface to 0.01 hPa (~ 80 km) and a horizontal resolution of $2.5^\circ \times 3.75^\circ$. The chemical

and source gas boundary conditions are similar to those used in the Chemistry-Climate Model Validation Activity for SPARC (CCMVal-2) REF0 simulation (Morgenstern et al., 2010).

Previous multi-dimensional modelling studies of MSP transport from the mesosphere to the stratosphere have treated microphysical processes such as Brownian coagulation and gravitational sedimentation (Megner et al., 2006, 2008; Bardeen et al., 2008). Sensitivity tests in the 3-D study of Bardeen et al. (2008) concluded that sedimentation is of secondary importance compared with vertical advection. Initial test runs with UMSLIMCAT where Brownian coagulation was included indicated no significant effect on the transport of MSP particle mass by advection. This is because sedimentation of these small particles, even after coagulation, is very slow. Consequently, MSPs were treated simply as an advective tracer of nominal (spherical) size subject to eddy diffusion and the calculated wind fields.

The tracer mixing ratio in the top level of UMSLIMCAT was held constant, set to a value (see below) calculated from the total particle number derived from the output of a 1-D particle growth/transport model (Saunders et al., 2007). The 1-D model is initiated using a chosen global meteoric mass influx ($t\,d^{-1}$) with particle transport driven by vertical eddy diffusion, and particle growth treated using parameterisations for both Brownian and magnetically driven coagulation (Saunders and Plane, 2006; Saunders et al., 2007). A mean tracer radius of ~ 1.5 nm (mass $= 2.8 \times 10^{-20}$ g, assumed particle density $= 2.0\,\mathrm{g\,cm^{-3}}$) was calculated from the 1-D output of total particle number and surface area. This is only slightly larger than the value of 1.3 nm chosen in the original 1-D modelling study of MSPs in the mesosphere and stratosphere (Hunten et al., 1980).

In UMSLIMCAT, particles were assumed to be removed at the Earth's surface by dry deposition. This was simulated by removing a nominal 10 % of particles in the lowest model level at each time step (1800 s); these particles were then stored as a non-advected tracer. The sensitivity of the model to the choice of fractional removal in the lowest level was tested by repeating runs with 1 % and 100 % removal per time step.

Changing the removal rate resulted in small ($< 5\%$) differences to the predicted particle numbers in the stratosphere and above (the region of interest in this study), whilst causing more significant differences ($> 50\%$) at altitudes below 12 km. All simulations were initialised with parameters for the year 2000, and were run for a total of five years following an initial five year spin-up period.

To investigate the impact of MSPs on H_2SO_4 removal above 35 km, the model H_2SO_4 concentration at 35 km was set at $5 \times 10^6\,cm^{-3}$, consistent with the mid-range of measurements at this altitude (Arnold et al., 1981; Viggiano and Arnold, 1981; Schlager and Arnold, 1987). The uptake of H_2SO_4 molecules on smoke particles was treated using first-order kinetics, such that the loss rate ($cm^{-3}\,s^{-1}$) is given by

$$\frac{d[H_2SO_4]}{dt} = -\frac{\bar{c}}{4}\gamma A[H_2SO_4] \tag{2}$$

where $\bar{c} = 1468 \times \sqrt{T}$ is the mean thermal velocity ($cm\,s^{-1}$) of an H_2SO_4 molecule at temperature T, γ is the heterogeneous uptake coefficient, and A is the volumetric particle surface area ($cm^2\,cm^{-3}$). Four simulations were performed using γ values ranging from zero to 0.01.

3.1 1-D modelling of MSP growth and transport

A number of runs were performed with the 1-D model using a varying meteoric mass input ($t\,d^{-1}$) in order to optimise the 3-D tracer input number concentration (mixing ratio) at 80 km for the purpose of matching (i) the reported meteoric metal content (0.5–1.0 Wt % Fe) in sampled SSA (Murphy et al., 1998; Cziczo et al., 2001) and (ii) measured particle extinction in the mesosphere and upper stratosphere (Hervig et al., 2009). The 1-D model was run in each case for a period of 5 yr to ensure a steady-state particle mass distribution throughout the full altitude range (110 km–20 km).

Figure 4 shows the altitude profile of the total (size integrated) MSP number concentration predicted with a daily meteoric input of 22 t, which results in 3000 particles cm^{-3} at 80 km. Similar profiles are obtained for other input rates with, for example, particle

numbers of 4000 and 2200 cm^{-3} at 80 km for 44 and 11 t d^{-1}, respectively. These MSP concentrations are typical of values reported from rocket-borne dust detector measurements in the upper mesosphere (Gelinas et al., 2005; Lynch et al., 2005; Rapp et al., 2007).

5   Results are shown for scenarios in which particle growth (starting from a "molecular" size particle of 0.3 nm radius) is treated assuming coagulation at all altitudes (red line), and then where the coagulation is turned off below 80 km (black line). Although the effect of coagulation is seen to significantly reduce particle numbers below 80 km in the 1-D model, this is due to the high number of small particles (radius < 1.5 nm)
10 which dominate the size distribution in the mesosphere. Advection processes treated in the 3-D model dominate the transport of such small particles, therefore making coagulation a comparatively unimportant process as verified in the initial test runs with UMSLIMCAT.

3.2   3-D modelling of MSP transport to the lower stratosphere

15 UMSLIMCAT was run with the MSP tracer concentration at 80 km fixed to 3000 cm^{-3}. Following spin up, the model was run for 5 years and the particle number density for the same month in each year averaged to remove year-to-year fluctuations. The resulting particle number density was then converted to the volumetric mass of MSP Fe (assuming an olivine composition of MgFeSiO$_4$), since this measure of MSP distribution
20 does not depend on the degree of particle coagulation (see above). Figure 5 shows the monthly mean Fe volumetric mass as a function of height and latitude for January, April, July and October. The downward transport of MSPs in the winter polar vortices from the mesosphere into the stratosphere is evident, as has been noted in previous modelling studies (Bardeen et al., 2008; Megner et al., 2008). MSPs are then redistributed to
25 lower latitudes in the stratosphere by the Brewer-Dobson circulation.

    Meteoric Fe was sampled in SSA by Cziczo et al. (2001) during the months of April and May, from aircraft flights which covered latitudes 9–46 ° N at altitudes up to 19 km

(see the red box outlined in the panel for April in Fig. 5). For the meteoric mass input rate of $22\,t\,d^{-1}$, a mean volumetric mass of meteoric Fe of $(1.2 \pm 0.4) \times 10^{-15}\,g\,cm^{-3}$ would be available for incorporation into SSA. Monthly zonal mean SSA surface area density data from the SAGE II satellite (Thomason et al., 1997) indicate a mean aerosol surface area of $(8 \pm 1) \times 10^{-9}\,cm^2\,cm^{-3}$ for the relevant latitudes and altitudes, which would provide a SSA mass of $1.1 \times 10^{-13}\,g\,cm^{-3}$ assuming a mean radius of 250 nm and density of $1.63\,g\,cm^{-3}$ (i.e. a 75 Wt % acid droplet). Therefore, if all of the meteoric Fe in MSPs is incorporated into available SSA, this would give a figure of 1.1 Wt % Fe which compares with 0.5–1.0 % reported by Cziczo et al. (2001).

3.3 MSP light extinction calculations

The SOFIE spectrometer on the NASA AIM (Aeronomy of Ice in the Mesosphere) satellite has a sufficiently high signal-to-noise to observe optical extinction by MSPs (Hervig et al., 2009). Particle extinction measurements (in units of km^{-1}) at a wavelength of 1.037 µm were made over the height range 40–75 km during June at 65° S. For comparison, the modelled extinction was calculated using the MSP number concentration profile from UMSLIMCAT shown in Fig. 4 (note the satisfactory agreement between the 1-D and 3-D model profiles in this figure). Rayleigh theory for the 1.5 nm radius particles was assumed, as well as an olivine ($MgFeSiO_4$) composition with real and imaginary refractive indices of 1.73 and 0.07 at 1.037 µm, respectively (Dorschner et al., 1995). At this particle size and for this composition, absorption is the dominant process with an associated cross section per particle of $7.5 \times 10^{-17}\,cm^2$, compared with the scattering cross-section of $2.0 \times 10^{-22}\,cm^2$.

Figure 6 shows reasonable agreement, with the SOFIE data being ~ 3 times greater than modelled at 40 km, and the modelled extinction being ~ 4 times greater at 75 km. Although these differences are relatively small in magnitude, the discrepancy above 50 km may reflect several factors (apart from systematic errors in the satellite measurements and model predicted particle distribution): (i) uncertainty in the chosen MSP composition; (ii) deviations in the particle refractive indices from the bulk values used

Title Page

Abstract | Introduction

Conclusions | References

Tables | Figures

|◄ | ►|

◄ | ►

Back | Close

Full Screen / Esc

Printer-friendly Version

Interactive Discussion

in the calculation; and (iii) deviation from spherical particle shape. Concerning points (i) and (ii), subsequent analysis of the SOFIE data at additional wavelengths indicates that the assumed olivine composition provides a best fit candidate compared with other possible MSP compositions (presentation by Mark Hervig, 38th COSPAR Scientific Assembly, Bremen, 2010). However, the fitting procedure necessarily assumes that the bulk refractive index is applicable to small nanoparticles (for which no such data currently exists) when determining the optical properties of MSPs. The size dependence at the nano-scale of the imaginary (absorption) index κ for a given particle composition has long been discussed with regard to interstellar dust grains (e.g. Huffman, 1977). Such effects could provide an explanation for the differences observed in Fig. 6 above 50 km. For example, reducing κ, whose bulk value is 0.07 at 1.037 µm, by a factor of 4 brings the calculated extinction into agreement with the SOFIE data point at 75 km.

Concerning point (iii), at lower altitudes the extinction measured by SOFIE most likely results from MSPs which have agglomerated to form non–spherical (fractal) morphologies (the red line in Fig. 4). To evaluate whether this could explain the modelled extinction below 50 km being lower than observed (Fig. 6), we conducted test calculations for aggregates composed of a varying number (N_p) of primary particles (radius r_p), with the fractal dimension D_f ranging from 1.5 to 2.0. Refractive indices were calculated using Maxwell–Garnett theory over a range of particle porosities ($P = 0.1$–0.9) (Saunders et al., 2007). The particle extinction was estimated using Mie theory with an effective (fractal) particle radius $r_f (= r_p \times N_p^{(1/Df)})$. There is no unique combination of D_f, N_p and P which provides a fit but, for example, for $D_f = 1.75$, $N_p = 8$ (giving a fractal radius of 4.9 nm), and $P = 0.5$ (complex refractive index $m = 1.37 - i0.04$), the SOFIE extinction at 40 km can be matched by the modelled extinction.

Another factor to consider is that the uptake of acids such as H_2SO_4 (see below) and water may cause the MSP size to increase (and perhaps also alter the refractive index). For example, increasing the tracer radius from 1.5 to just 2.2 nm, but maintaining the number density, would also provide a match to the SOFIE extinction at 40 km.

3.4 3-D modelling results of MSP-H_2SO_4 interactions in the stratosphere

Using a tracer concentration based on the $22\,t\,d^{-1}$ mass input, UMSLIMCAT was run to investigate H_2SO_4 loss on MSPs. Figure 7 shows the corresponding profile of predicted H_2SO_4 concentrations at $44°\,N$ (from where all measured data is reported) from above 30 km for $\gamma = 0$, 10^{-4}, 10^{-3} and 0.01 as indicated in the legend. At 45 km, the $\gamma = 0.01$ data falls within the measured data error bar with $[H_2SO_4]$ set to $5 \times 10^6\,cm^{-3}$ at 35 km, which is in the middle of the measured range (shown by the coloured points in Fig. 7). It is clear that γ would need to be greater than 0.01 if heterogeneous acid loss to particles is the sole significant depletion process for H_2SO_4 in the upper stratosphere.

A final point is whether there are actually sufficient metal atoms in MSPs to remove the adsorbed H_2SO_4. The number of metal atoms present in MSPs between 30 and 45 km can be compared with the H_2SO_4 concentration profile when $\gamma = 0$ (i.e. no smoke present). Assuming a molecular olivine radius of 0.3 nm, the 1.5 nm radius tracer particle would contain 125 molecules. Therefore at 45 km, from the predicted MSP number, the total number of metal (Fe + Mg) atoms is $1.1 \times 10^7\,cm^{-3}$ – equivalent to a mixing ratio of $\sim 2.2 \times 10^{-10}$. This compares with an acid mixing ratio of $\sim 8 \times 10^{-11}$ at the same altitude i.e. an excess of metal atoms would be available in the upper stratosphere for the heterogeneous removal of H_2SO_4. This ratio of 2.8 decreases at lower altitudes to below 2.0 at ~ 42 km (consistent with increasing acid levels) and to 0.6 at 30 km.

4 Discussion and atmospheric implications

4.1 Dissolution of MSPs in H_2SO_4/H_2O mixtures

The measured rate coefficients (k) describe the overall rate of a complex mechanism of competing processes which convert Fe^{2+} in solid silicate particles to Fe^{3+} species in solution. Although the rate-limiting step is not explicitly identified, the observed trends in k suggest that, due to increased solution viscosity at lower temperatures/higher

Wt % acid, the diffusion of H_2SO_4 molecules to the particle surface is an important controlling factor. Oxidation of Fe^{2+} to Fe^{3+} under such highly acidic conditions is likely to be rapid, and the observation that the ratio of bare Fe^{3+} to complexed Fe^{3+} (measured by the ratio of absorbance peaks in the spectra) was constant during the course of the reaction indicates that the dissolution and ion-complexation processes are also fast. There has been much discussion in the literature regarding the mechanisms of silicate mineral weathering e.g. (Schott and Berner, 1983; Casey and Westrich, 1992; Liu et al., 2006).

The amorphous silicate powders displayed significantly faster dissolution compared with crystalline Fe^{2+} compounds. For example, experiments with Mohr's salt added to a 75 % Wt acid solution, indicated that after 24 h, < 10 % of the Fe^{2+} had been converted to Fe^{3+}. The lower solubility/dissolution of crystalline compounds is consistent with the study of Wise et al. (2003), although their conclusion that Fe^{2+} is the exclusive species remaining in solution is contradicted by the spectral analysis in the present study. Clearly, a distinct structural effect is evident, with an amorphous particle form promoting faster reaction and dissolution. This was further verified by a comparison of the dissolution rates of high purity amorphous and crystalline ferric oxide (Fe_2O_3) powders. The former, synthesised in our laboratory via a photo-oxidation method (Saunders and Plane, 2006), was found to result in 100 % dissolution within 12 h in a 75 % Wt solution at 295 K, whereas a commercial crystalline sample exhibited only ∼ 20 % dissolution after 24 h under the same conditions. The disparity in dissolution rates between crystalline and amorphous compounds is also consistent with the reported enhanced solubility of amorphous silica (SiO_2) at $T \geq 273$ K compared with that of crystalline quartz e.g. (Gunnarsson and Arnorsson, 2000).

The observed dissolution rates of the amorphous meteoric smoke analogue powders in H_2SO_4-H_2O solutions at temperatures down to 223 K indicate that the dissolution of MSPs within SSA in the Junge layer will occur within a few days. Prior to dissolution, the collision between an MSP and an SSA with radii of 1.5 nm and 250 nm, respectively, resulting purely from Brownian motion under conditions relevant to the

Title Page

Abstract | Introduction

Conclusions | References

Tables | Figures

◄ | ►

◄ | ►

Back | Close

Full Screen / Esc

Printer-friendly Version

Interactive Discussion

lower stratosphere, would take ~ 2 days (coagulation kernel $\beta \sim 3.4 \times 10^{-6}\,\mathrm{cm^3\,s^{-1}}$ – see Eq. (E2) in Saunders and Plane, 2006, and assuming a typical SSA number concentration of $2\,\mathrm{cm^{-3}}$).

The greater observed solubility/dissolution of amorphous Fe^{2+} minerals, compared with those of a crystalline nature, suggests that more of the Fe-content within stratospheric aerosol is likely to be in the form of soluble bare or sulphate-complexed Fe^{3+} ions (stabilised against conversion to solid-phase iron oxide/hydroxide species by the low temperature/low pH environment within the droplets). One possible ramification of such enhanced particle solubilities within supercooled SSA would be a reduced potential for MSPs to remain as solid particles and nucleate PSCs below 200 K, at the low saturation ratios proposed by (Voigt et al., 2005). Conversely, an enhanced free (cation) or complexed metal anion composition within SSA could provide an increased role for the ion-induced nucleation of such species.

4.2 Removal of H_2SO_4 in the upper stratosphere/lower mesosphere

The rate of input of interplanetary dust particles to the Earth's atmosphere has been the subject of much recent debate, with estimates ranging from $\sim 5\text{–}300\,\mathrm{t\,d^{-1}}$ (Vondrak et al., 2008). Our optimised level of $22\,\mathrm{t\,d^{-1}}$, used to account for the measured metal content in SSA and for fitting the observed particle extinction from the upper stratosphere to the mesosphere, fixes this crucial parameter at the lower end of the currently accepted range.

To our knowledge, there are currently no reported laboratory measurements of the uptake of H_2SO_4 onto aerosol of a meteoritic nature. Hence, our conclusion from the modelling exercise that $\gamma \geq 0.01$ should now be tested in the laboratory using appropriate MSP mimics under stratospheric conditions. Reports of the measured uptake of acids such as HNO_3 onto mineral (crystalline) dust samples indicate a wide range of uptake coefficient values ($10^{-8} < \gamma < 0.5$), reflecting the differences in particle size/composition/morphology and in the techniques and conditions employed (see

Title Page

Abstract	Introduction
Conclusions	References
Tables	Figures

|◄ | ►|

◄ | ►

Back | Close

Full Screen / Esc

Printer-friendly Version

Interactive Discussion

This indicates the critical importance of closely replicating materials and conditions for future laboratory measurements of H_2SO_4 uptake on MSP analogues under stratospheric conditions.

5 Conclusions

Spectroscopic measurements of the acid dissolution of synthesised amorphous iron-rich olivine powders in H_2SO_4 solutions of 30–75 Wt%, and at temperatures of 223–295 K, indicate complete conversion to soluble Fe^{3+} ions (bare and complexed) under all conditions. The dissolution rate decreases with increasing acid Wt% and lower temperature. For the most extreme conditions amenable to our laboratory analysis (75 Wt% acid/223 K), corresponding to the mid-latitude stratosphere, it is predicted that meteoric smoke particles will fully dissolve in the stratospheric aerosol layer within a week.

Modelling the transport of MSPs from the upper mesosphere to the troposphere indicates that a meteoric mass input rate of about $20\,t\,d^{-1}$ would result in a Fe content in stratospheric aerosol that matches the samples collected in the lower stratosphere. The same input also gives a sensible fit to measured particle extinction values from the upper stratosphere to the mesosphere. Of course, this mass input rate depends on the assumptions made about the MSP size and number density in the upper mesosphere, as well as transport in the model, and so is quite uncertain (by at least a factor of 2). At this flux, the model indicates that a heterogeneous uptake coefficient (γ) of 0.01 or larger for loss of H_2SO_4 vapour on MSPs would be required to account for the observed two orders of magnitude depletion of the acid in the upper stratosphere.

References

Arijs, E., Nevejans, D., Ingels, J., and Frederick, P.: Negative-ion composition and sulfuric-acid vapor in the upper-stratosphere, Planet. Space Sci., 31, 1459–1464, 1983.

Arijs, E., Nevejans, D., Ingels, J., and Frederick, P.: Recent stratospheric negative-ion composition measurements between 22-km and 45-km altitude, J. Geophys. Res., 90, 5891–5896, 1985.

Arnold, F., Fabian, R., and Joos, W.: Measurements of the height variation of sulfuric-acid vapor concentrations in the stratosphere, Geophys. Res. Lett., 8, 293–296, 1981.

Bardeen, C. G., Toon, O. B., Jensen, E. J., Marsh, D. R., and Harvey, V. L.: Numerical simulations of the three-dimensional distribution of meteoric dust in the mesosphere and upper stratosphere, J. Geophys. Res., 113, D17202, doi:10.1029/2007JD009515, 2008.

Biermann, U. M., Presper, T., Koop, T., Mossinger, J., Crutzen, P. J., and Peter, T.: The unsuitability of meteoritic and other nuclei for polar stratospheric cloud freezing, Geophys. Res. Lett., 23, 1693–1696, 1996.

Burns, R. G.: Ferric sulfates on mars, J. Geophys. Res., 92, 570–574, 1987.

Burns, R. G.: Rates and mechanisms of chemical-weathering of ferromagnesian silicate minerals on mars, Geochim. Cosmochim. Acta, 57, 4555–4574, 1993.

Carslaw, K. S., Peter, T., and Clegg, S. L.: Modeling the composition of liquid stratospheric aerosols, Rev. Geophys., 35, 125–154, 1997.

Casey, W. H. and Westrich, H. R.: Control of dissolution rates of orthosilicate minerals by divalent metal oxygen bonds, Nature, 355, 157–159, 1992.

Chipperfield, M. P.: New version of the tomcat/slimcat off-line chemical transport model: intercomparison of stratospheric tracer experiments, Q. J. Roy. Met. Soc., 132, 1179–1203, 2006.

Curtius, J., Weigel, R., Vössing, H.-J., Wernli, H., Werner, A., Volk, C.-M., Konopka, P., Krebsbach, M., Schiller, C., Roiger, A., Schlager, H., Dreiling, V., and Borrmann, S.: Observations of meteoric material and implications for aerosol nucleation in the winter Arctic lower stratosphere derived from in situ particle measurements, Atmos. Chem. Phys., 5, 3053–3069, doi:10.5194/acp-5-3053-2005, 2005.

Cziczo, D. J., Thomson, D. S., and Murphy, D. M.: Ablation, flux, and atmospheric implications of meteors inferred from stratospheric aerosol, Science, 291, 1772–1775, 2001.

Deshler, T.: A review of global stratospheric aerosol: measurements, importance, life cycle,

Title Page

Abstract | Introduction

Conclusions | References

Tables | Figures

◄ | ►

◄ | ►

Back | Close

Full Screen / Esc

Printer-friendly Version

Interactive Discussion

and local stratospheric aerosol, Atmos. Res., 90, 223–232, 2008.

Dorschner, J., Begemann, B., Henning, T., Jager, C., and Mutschke, H.: Steps toward interstellar silicate mineralogy. 2. Study of mg-fe-silicate glasses of variable composition, Astron. Astrophys., 300, 503–520, 1995.

5 Draine, B. T.: Interstellar dust grains, Ann. Rev. Astron. Astroph., 41, 241–289, 2003.

Gelinas, L. J., Lynch, K. A., Kelley, M. C., Collins, R. L., Widholm, M., MacDonald, E., Ulwick, J., and Mace, P.: Mesospheric charged dust layer: Implications for neutral chemistry, J. Geophys. Res., 110, A01310, doi:10.1029/2004JA010503, 2005.

Gumbel, J. and Megner, L.: Charged meteoric smoke as ice nuclei in the mesosphere: Part 1

10 – a review of basic concepts, J. Atmos. Solar-Terr. Phys., 71, 1225–1235, 2009.

Gunnarsson, I. and Arnorsson, S.: Amorphous silica solubility and the thermodynamic properties of H_4SiO_4 degrees in the range of 0 °C to 350 °C at p_{sat}, Geochim. Cosmochim. Acta, 64, 2295–2307, 2000.

Hervig, M. E., Gordley, L. L., Deaver, L. E., Siskind, D. E., Stevens, M. H., Russell, J. M.,

15 Bailey, S. M., Megner, L., and Bardeen, C. G.: First satellite observations of meteoric smoke in the middle atmosphere, Geophys. Res. Lett., 36, L18805, doi:10.1029/2009GL039737, 2009.

Hochella, M. F., Lower, S. K., Maurice, P. A., Penn, R. L., Sahai, N., Sparks, D. L., and Twining, B. S.: Nanominerals, mineral nanoparticles, and earth systems, Science, 319, 1631–

20 1635, 2008.

Huffman, D. R.: Interstellar grains – interaction of light with a small-particle system, Adv. Phys., 26, 129–230, 1977.

Hunten, D. M., Turco, R. P., and Toon, O. B.: Smoke and dust particles of meteoric origin in the mesosphere and stratosphere, J. Atmos. Sci., 37, 1342–1357, 1980.

25 Hurowitz, J. A., McLennan, S. M., Tosca, N. J., Arvidson, R. E., Michalski, J. R., Ming, D. W., Schroder, C., and Squyres, S. W.: In situ and experimental evidence for acidic weathering of rocks and soils on mars, J. Geophys. Res., 111, E02S19, doi:10.1029/2005JE002515, 2006.

Liu, Y., Olsen, A. A., and Rimstidt, J. D.: Mechanism for the dissolution of olivine series minerals

30 in acidic solutions, Amer. Mineral., 91, 455–458, 2006.

Loughnan, F. C.: Chemical Weathering of the Silicate Minerals, Elsevier, New York, 1969.

Lynch, K. A., Gelinas, L. J., Kelley, M. C., Collins, R. L., Widholm, M., Rau, D., MacDonald, E., Liu, Y., Ulwick, J., and Mace, P.: Multiple sounding rocket observations of charged dust in

Title Page

Abstract | Introduction

Conclusions | References

Tables | Figures

◄ | ►

◄ | ►

Back | Close

Full Screen / Esc

Printer-friendly Version

Interactive Discussion

the polar winter mesosphere, J. Geophys. Res., 110, A03302, doi:10.1029/2004JA010502, 2005.

Megner, L., Rapp, M., and Gumbel, J.: Distribution of meteoric smoke – sensitivity to microphysical properties and atmospheric conditions, Atmos. Chem. Phys., 6, 4415–4426, doi:10.5194/acp-6-4415-2006, 2006.

Megner, L., Siskind, D. E., Rapp, M., and Gumbel, J.: Global and temporal distribution of meteoric smoke: a two-dimensional simulation study, J. Geophys. Res., 113, D03202, doi:10.1029/2007JD009054, 2008.

Mills, M. J., Toon, O. B., Vaida, V., Hintze, P. E., Kjaergaard, H. G., Schofield, D. P., and Robinson, T. W.: Photolysis of sulfuric acid vapor by visible light as a source of the polar stratospheric CN layer, J. Geophys. Res., 110, D08201, doi:10.1029/2004JD005519, 2005.

Morgenstern, O., Giorgetta, M. A., Shibata, K., Eyring, V., Waugh, D. W., Shepherd, T. G., Akiyoshi, H., Austin, J., Baumgaertner, A. J. G., Bekki, S., Braesicke, P., Bruhl, C., Chipperfield, M. P., Cugnet, D., Dameris, M., Dhomse, S., Frith, S. M., Garny, H., Gettelman, A., Hardiman, S. C., Hegglin, M. I., Jockel, P., Kinnison, D. E., Lamarque, J. F., Mancini, E., Manzini, E., Marchand, M., Michou, M., Nakamura, T., Nielsen, J. E., Olivie, D., Pitari, G., Plummer, D. A., Rozanov, E., Scinocca, J. F., Smale, D., Teyssedre, H., Toohey, M., Tian, W., and Yamashita, Y.: Review of the formulation of present-generation stratospheric chemistry-climate models and associated external forcings, J. Geophys. Res., 115, D00M02, doi:10.1029/2009JD013728, 2010.

Murphy, D. M., Thomson, D. S., and Mahoney, T. M. J.: In situ measurements of organics, meteoritic material, mercury, and other elements in aerosols at 5 to 19 kilometers, Science, 282, 1664–1669, 1998.

Neely III, R. R., English, J. M., Toon, O. B., Solomon, S., Mills, M., and Thayer, J. P.: Implications of extinction due to meteoritic smoke in the upper stratosphere, Geophys. Res. Lett., 38, L24808, doi:10.1029/2011GL049865, 2011.

Plane, J. M. C.: Atmospheric chemistry of meteoric metals, Chem. Rev., 103, 4963–4984, 2003.

Potterill, R. H., Walker, O. J., Weiss, J.: Electron affinity spectrum of ferrous ion in aqueous solution, Proc. Roy. Soc. London A, 156, 561–570, 1936.

Prather, M. J. and Rodriguez, J. M.: Antarctic ozone – meteoric control of HNO_3, Geophys. Res. Lett., 15, 1–4, 1988.

Rapp, M. and Thomas, G. E.: Modeling the microphysics of mesospheric ice particles: assess-

Title Page

Abstract | Introduction

Conclusions | References

Tables | Figures

|◄ | ►|

◄ | ►

Back | Close

Full Screen / Esc

Printer-friendly Version

Interactive Discussion

ment of current capabilities and basic sensitivities, J. Atmos. Solar-Terr. Phys., 68, 715–744, 2006.

Rapp, M., Strelnikova, I., and Gumbel, J.: Meteoric smoke particles: evidence from rocket and radar techniques, Adv. Space Res., 40, 809–817, 2007.

5 Saunders, R. W. and Plane, J. M. C.: A laboratory study of meteor smoke analogues: composition, optical properties and growth kinetics, J. Atmos. Solar-Terr. Phys., 68, 2182–2202, 2006.

Saunders, R. W. and Plane, J. M. C.: A photo-chemical method for the production of olivine nanoparticles as cosmic dust analogues, Icarus, 212, 373–382, 2011.

10 Saunders, R. W., Forster, P. M., and Plane, J. M. C.: Potential climatic effects of meteoric smoke in the Earth's paleo-atmosphere, Geophys. Res. Lett., 34, L16801, doi:10.1029/2007GL029648, 2007.

Scharf, K. and Lee, R. M.: Investigation of spectrophotometric method of measuring ferric ion yield in ferrous sulfate dosimeter, Radiation Res., 16, 115, 1962.

15 Schlager, H. and Arnold, F.: Balloon-borne composition measurements of stratospheric negative-ions and inferred sulfuric-acid vapor abundances during the map-globus 1983 campaign, Planet. Space Sci., 35, 693–701, 1987.

Schott, J. and Berner, R. A.: X-ray photoelectron studies of the mechanism of iron silicate dissolution during weathering, Geochim. Cosmochim. Acta, 47, 2233–2240, 1983.

20 Siever, R. and Woodford, N.: Dissolution kinetics and the weathering of mafic minerals, Geochim. Cosmochim. Acta, 43, 717–724, 1979.

Stopar, J. D., Taylor, G. J., Hamilton, V. E., and Browning, L.: Kinetic model of olivine dissolution and extent of aqueous alteration on mars, Geochim. Cosmochim. Acta, 70, 6136–6152, 2006.

25 Thomason, L. W., Poole, L. R., and Deshler, T.: A global climatology of stratospheric aerosol surface area density deduced from stratospheric aerosol and gas experiment II measurements: 1984–1994, J. Geophys. Res., 102, 8967–8976, 1997.

Thompson, S. P., Evans, A., and Jones, A. P.: Structural evolution in thermally processed silicates, Astron. Astrophys., 308, 309–320, 1996.

30 Tian, W. S., and Chipperfield, M. P.: A new coupled chemistry-climate model for the stratosphere: the importance of coupling for future O-3-climate predictions, Q. J. Roy. Met. Soc., 131, 281–303, 2005.

Turco, R. P., Toon, O. B., Hamill, P., and Whitten, R. C.: Effects of meteoric debris on strato-

spheric aerosols and gases, J. Geophys. Res., 86, 1113–1128, 1981.

Vaida, V., Kjaergaard, H. G., Hintze, P. E., and Donaldson, D. J.: Photolysis of sulfuric acid vapor by visible solar radiation, Science, 299, 1566–1568, 2003.

Viggiano, A. A. and Arnold, F.: Extended sulfuric-acid vapor concentration measurements in the stratosphere, Geophys. Res. Lett., 8, 583–586, 1981.

Voigt, C., Schlager, H., Luo, B. P., Dörnbrack, A., Roiger, A., Stock, P., Curtius, J., Vössing, H., Borrmann, S., Davies, S., Konopka, P., Schiller, C., Shur, G., and Peter, T.: Nitric Acid Tri-hydrate (NAT) formation at low NAT supersaturation in Polar Stratospheric Clouds (PSCs), Atmos. Chem. Phys., 5, 1371–1380, doi:10.5194/acp-5-1371-2005, 2005.

Vondrak, T., Plane, J. M. C., Broadley, S., and Janches, D.: A chemical model of meteoric ablation, Atmos. Chem. Phys., 8, 7015–7031, doi:10.5194/acp-8-7015-2008, 2008.

White, A. F. and Brantley, S. L.: Chemical weathering rates of silicate minerals, in: Reviews in Mineralogy, edited by: Ribbe, P. H., Mineralogical Society of America, Washington, 1995.

Whiteker, R. A. and Davidson, N.: Ion-exchange and spectrophotometric investigation of iron(ii) sulfate complex ions, J. Am. Chem. Soc., 75, 3081–3085, 1953.

Williams, L. R. and Long, F. S.: Viscosity of supercooled sulfuric-acid-solutions, J. Phys. Chem., 99, 3748–3751, 1995.

Wise, M. E., Brooks, S. D., Garland, R. M., Cziczo, D. J., Martin, S. T., and Tolbert, M. A.: Solubility and freezing effects of Fe^{2+} and Mg^{2+} in H_2SO_4 solutions representative of upper tropospheric and lower stratospheric sulfate particles, J. Geophys. Res., 108, 4434, doi:10.1029/2003JD003420, 2003.

Interactions of meteoric smoke particles with sulphuric acid

R. W. Saunders et al.

Title Page

Abstract | Introduction

Conclusions | References

Tables | Figures

◀◀ | ▶▶

◀ | ▶

Back | Close

Full Screen / Esc

Printer-friendly Version

Interactive Discussion

Table 1. Measured activation energies (E_a) and pre-exponential factors (A) for the reaction rate coefficient for the dissolution of amorphous fayalite (Fe_2SiO_4) powder in H_2SO_4/H_2O solutions of varying Wt%.

Wt% acid solution	$E_a/\mathrm{kJ\,mol^{-1}}$	$\ln A$
30	27.6	7.079
40	34.2	9.671
50	42.1	12.985
60	49.9	16.050
75	59.9	21.200

10 μm
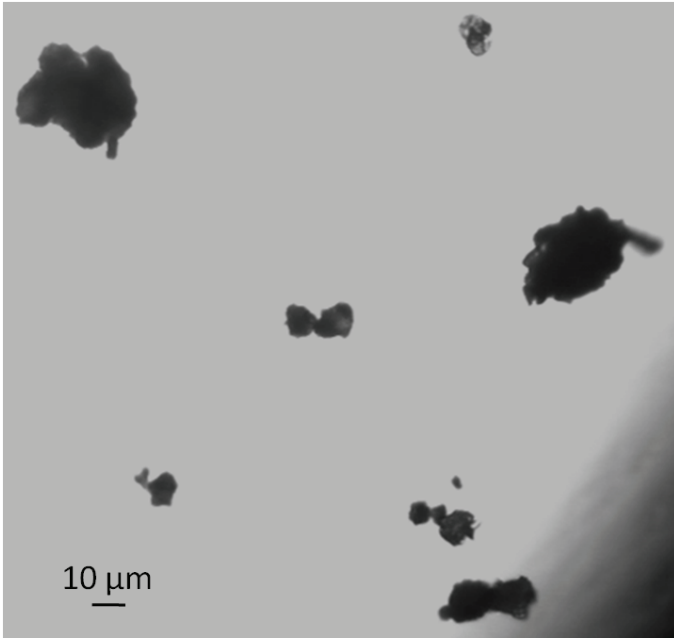
Fig. 1. Optical microscope image of synthesised silicate particles used in the acid solution-powder experiments.
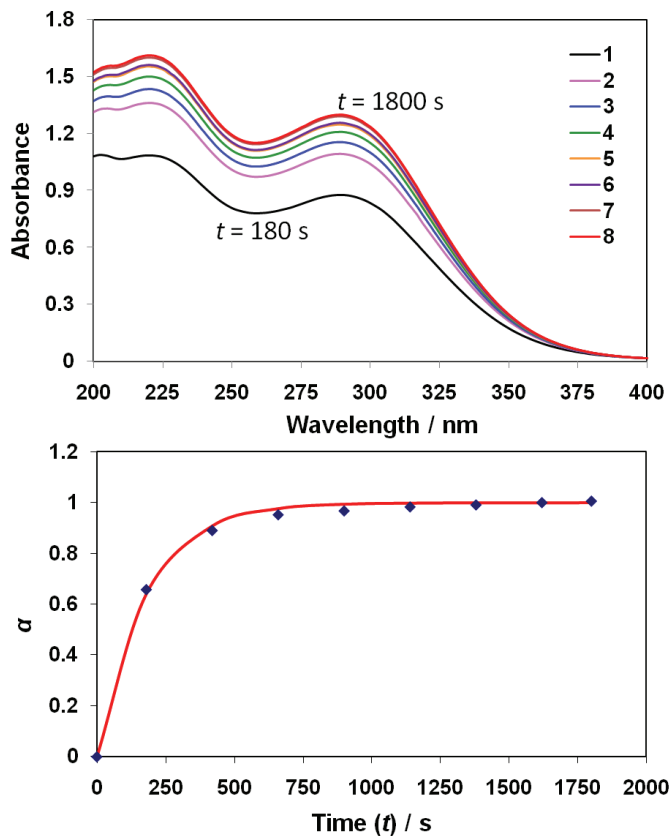
Fig. 2. The top panel shows a time series of UV-visible spectra taken from a 75% Wt H_2SO_4 solution at 273 K, to which amorphous fayalite powder had been added. The time at which each numbered (consecutive) spectrum was taken is indicated in the bottom panel, which is a plot of the ratio (α) of measured absorbance at the 289 nm ($Fe[SO_4]_2^-$) peak to the maximum (final) absorbance at time (t).
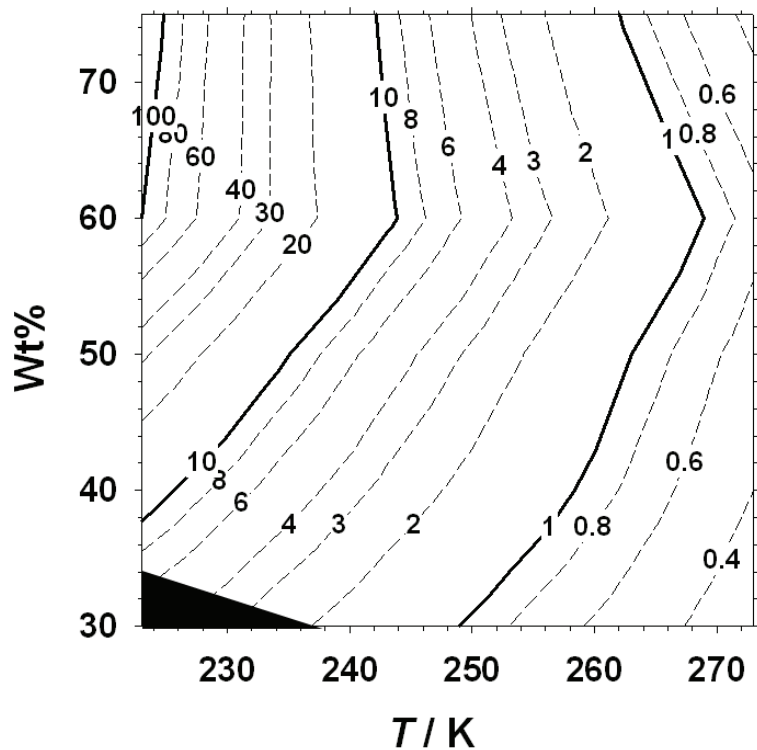
Fig. 3. Contour plots showing the calculated time in hours for the dissolution (> 99 %) of Fe^{2+} ions from fayalite powder as a function of temperature (223–273 K) and Wt% acid solution (30–75 %). The black shaded area indicates the conditions under which hexagonal water-ice (Ih) formation occurs in H$_2$SO$_4$-H$_2$O solutions.

Title Page

Abstract | Introduction

Conclusions | References

Tables | Figures

|◄ | ►|

◄ | ►

Back | Close

Full Screen / Esc

Printer-friendly Version

Interactive Discussion
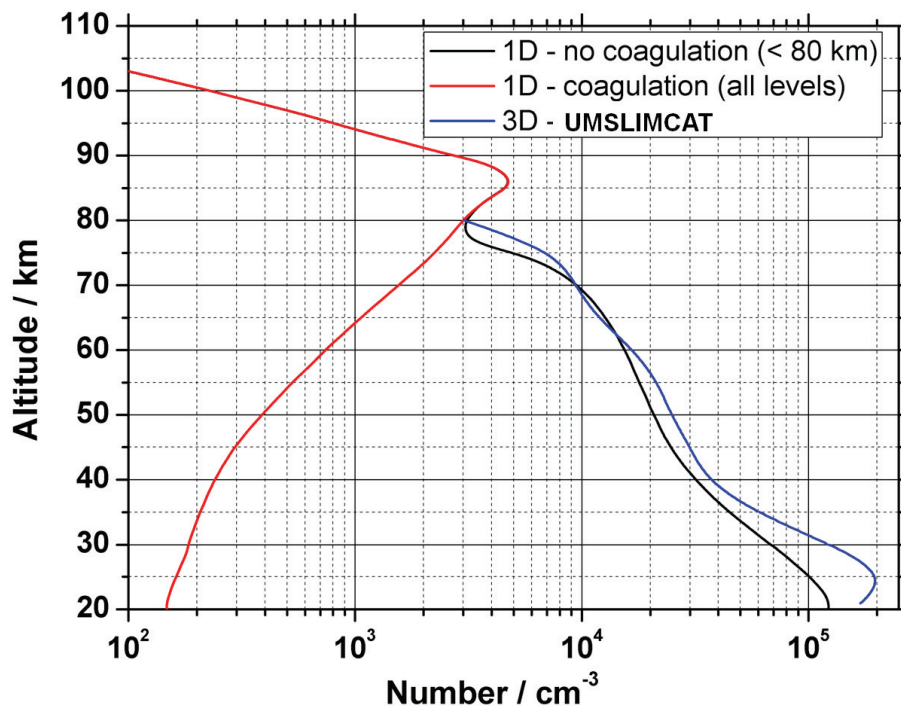
Fig. 4. Vertical profiles of the MSP concentration predicted by the 1-D model for the case where there is coagulation below 80 km (red line) or coagulation is switched off (black line). The global meteoric mass input rate is $22\,\mathrm{t\,d^{-1}}$. The blue line shows the MSP density profile calculated by UMSLIMCAT for June at 65° S.
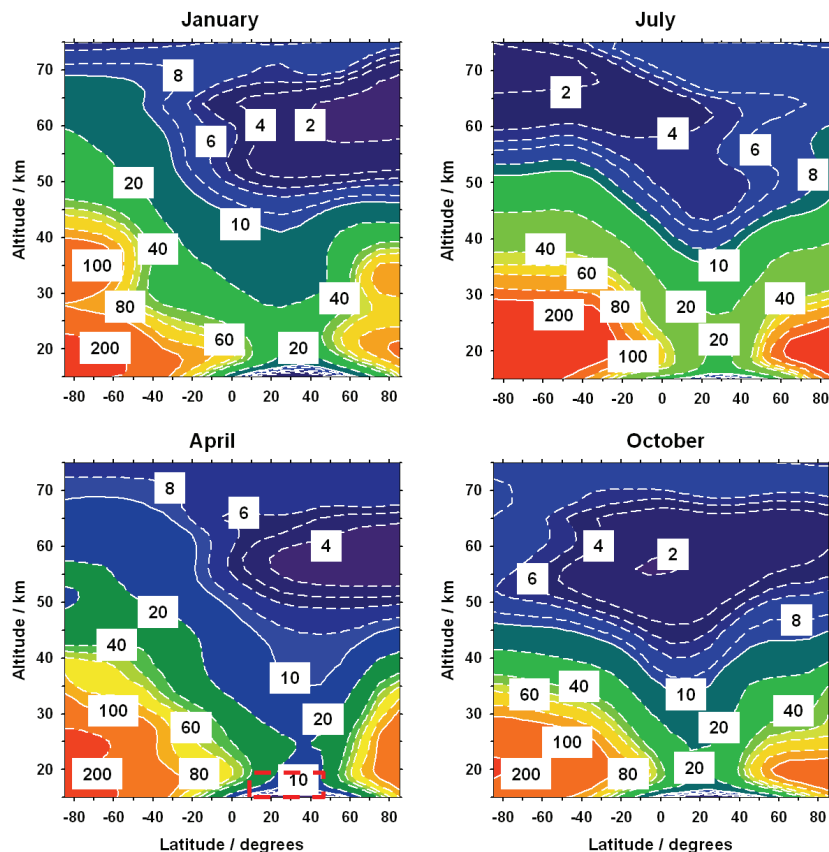
Fig. 5. Volumetric mass of MSP Fe ($\times 10^{-17}$ g cm^{-3}) calculated from the monthly mean MSP number densities from 2000–2005, predicted by UMSLIMCAT (global meteoric mass input rate = 22 t d^{-1}). The dashed outlined box in the plot for April indicates altitude and latitude ranges relevant to the measurements of Fe content in SSA (see text).

Title Page

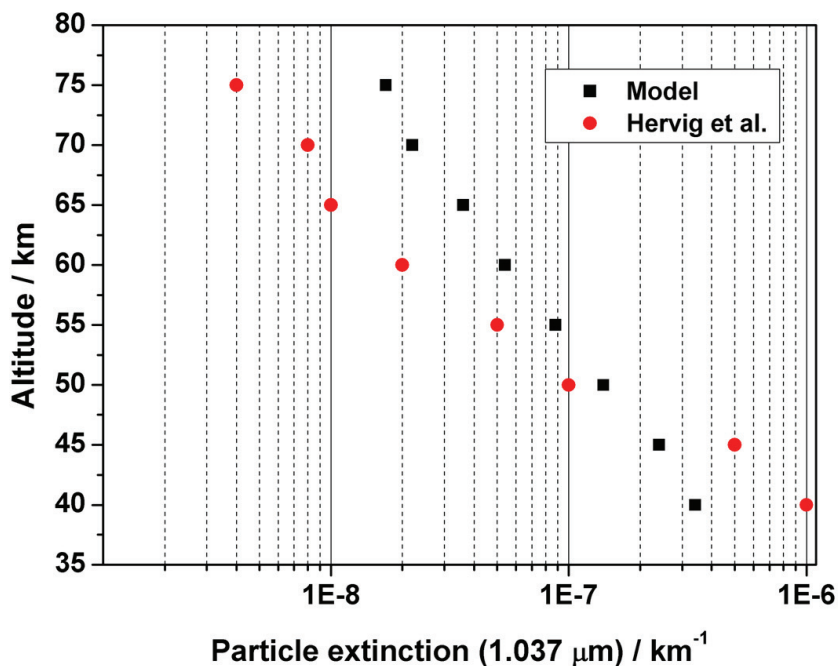Abstract · Introduction

Conclusions · References

Tables · Figures

|◄ · ►|

◄ · ►

Back · Close

Full Screen / Esc

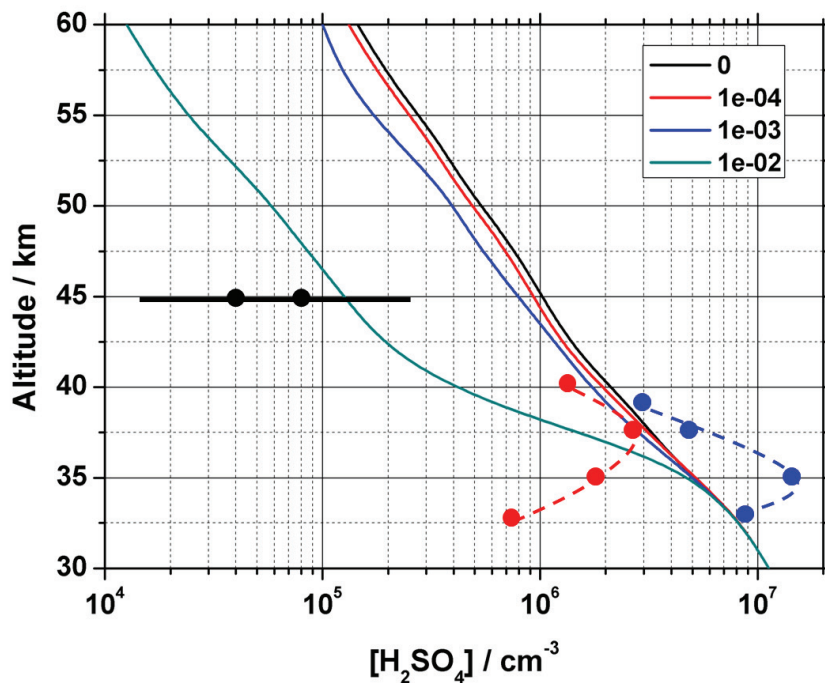Printer-friendly Version

Interactive Discussion

Fig. 6. Comparison of measured MSP extinction (Hervig et al., 2009) with values calculated using MSP number concentrations from the UMSLIMCAT model and Rayleigh theory for an assumed olivine (MgFeSiO$_4$) composition.

Fig. 7. Altitude profiles at 44° N of the H_2SO_4 concentration modelled in UMSLIMCAT with the heterogeneous uptake coefficients (γ) of H_2SO_4 on MSPs indicated in the legend. The solid points are balloon-borne measurements (blue – Viggiano and Arnold, 1981; red – Schlager and Arnold, 1987; black, with error bar – Arijs et al., 1985).